Applied Catalysis B: Environmental 198 (2016) 508–515

Contents lists available at ScienceDirect

Applied Catalysis B: Environmental

journal homepage: www.elsevier.com/locate/apcatb

Theoretical analyses of organic acids assisted surface-catalyzed reduction of Cr^{VI} on TiO_2 nanowire arrays

Lixia Yang[a], Ming Liu[a], Yuan Liu[a], Shenglian Luo[a,*], Yan Luo[a], Xubiao Luo[a], Guifa Li[b], Ping Peng[c]

[a] High Level Laboratory of Jiangxi Province for Persistent Pollutants Control, Recycle and Reuse, Nanchang Hangkong University, Nanchang 330063, PR China
[b] College of Material Science and Engineering, Nanchang Hangkong University, Nanchang 330063, PR China
[c] School of Materials Science and Engineering, Hunan University, Hunan 410082, PR China

ARTICLE INFO

Article history:
Received 5 December 2015
Received in revised form 17 May 2016
Accepted 1 June 2016
Available online 2 June 2016

Keywords:
Theoretical calculations
Cr^{VI} reduction
TiO_2 nanowires
Tartaric acid
Tartaric acid segment

ABSTRACT

Assisted by low molecular weight organic acids (LOAs), photocatalytic reduction of Cr^{VI} was studied in the presence of TiO_2 nanowire arrays (NWs) under the visible light. Theoretical calculations indicates that the decisive factors for this conversion are the stable adsorption behavior of LOA on TiO_2 and orbital overlapping between the LOA HOMO and TiO_2 LUMO. The orbital configuration interprets that covalent bonds are formed between the LOA and TiO_2. Direct electron transfer occurs from LOA to TiO_2 surface which facilitates the reducing of Cr^{VI}. Tartaric acid (TA) is proved to be the optimum organic acid for the surface-catalyzed reduction of Cr^{VI}. The TA can be easily excited by the light with wavelength higher than 1033 nm and be broken into two same molecular segments. The molecular segments accelerate the Cr^{VI} reduction which follows a two-stage pseudo-first-order kinetics that is slow at initial stage and fast at the second stage.

© 2016 Elsevier B.V. All rights reserved.

1. Introduction

As one of the most toxic and important heavy metals, Chromium (VI) is commonly detected in wastewater from industrial activities of tanning, electroplating and pigmenting. It is an acute carcinogen and more mobile and toxic than chromium (III). Increasing accumulation of Cr^{VI} in groundwater will be a significant environmental hazard. People will suffer chronic ulcer, dermatitis, corrosive reaction in nasal septum and local effects in lungs when there is excess Cr^{VI} in the body [1]. As a result, reduction of Cr^{VI} to Cr^{III} is of great importance in the view of environmental security. Early in 1996, Stong group [2] found that redox reaction could happen slowly between Cr^{VI} and some organic compounds such as hydroxylcarboxylic acids, esters with carbonyl carboxylic acid and substituted phenols under low pH conditions. They also found that the reduction of Cr^{VI} can be dramatically enhanced in the presence of TiO_2 because of the strong Lewis acid properties of TiO_2 [3]. Since then a lot of photocatalytic reduction research of Cr^{VI} under simulated solar light were carried out over Cr-TiO_2 systems [4–11]. Wang et al. reports an effective reduction of Cr^{VI} under visible light in the presence of LOAs [9]. They reported that LOAs with high highest occupied molecular orbital (E_{HOMO}) and low adiabatic ionization potential (AIP) could enhance the photocatalytic reduction activity of Cr^{VI}. In addition, the adsorption of LOAs on the TiO_2 surface governs the photocatalytic reduction efficiency of Cr^{VI}. However the theoretical understanding of the interactions and electron transfer behavior between LOAs and TiO_2 for the reduction of Cr^{VI} is lacking [12–14].

In this work, the adsorption of six LOAs on TiO_2 was simulated and the electron cloud between the LOAs and TiO_2 were visually exhibited for the first time. The six LOAs are formic acid (FA), oxalic acid (OA), succinic acid (SA), malic acid (MA), citric acid (CA) and tartaric acid (TA). They are grouped into carboxylic acids (FA, MA and OA) and α-hydroxyl carboxylic acids (CA, MA and TA). The stable absorption model of LOAs on TiO_2 were established and the electron densities between LOAs and TiO_2 were calculated. The calculation results illustrate that the TA molecule is easily cracked into two same segments. The TA segments (TAS) were tightly adsorbed on the surface of TiO_2, forming a very stable covalent bond with TiO_2 named TAS-TiO_2 species and the TAS are strong electron donors for TiO_2. The Cr^{VI} existing in $HCrO_4^-$ and CrO_4^{2-} forms was absorbed on the TiO_2 surface too and accepted the electrons from the TiO_2 CB to be reduced. Strong electronic coupling between the TiO_2 substrate and the LOA was key for the electron transfer. The

* Corresponding author.
E-mail address: sllou@hnu.edu.cn (S. Luo).

http://dx.doi.org/10.1016/j.apcatb.2016.06.002
0926-3373/© 2016 Elsevier B.V. All rights reserved.

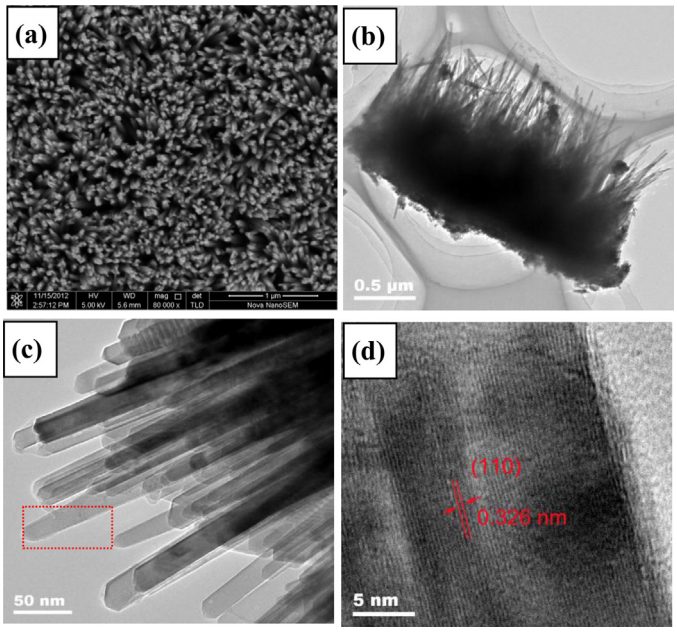

Fig. 1. (a) SEM image of as-prepared TiO_2 nanowire arrays, (b) TEM image showing whole lateral view of the nanowire arrays, (c) and (d) TEM image depicting the detailed morphologies of the nanowires.

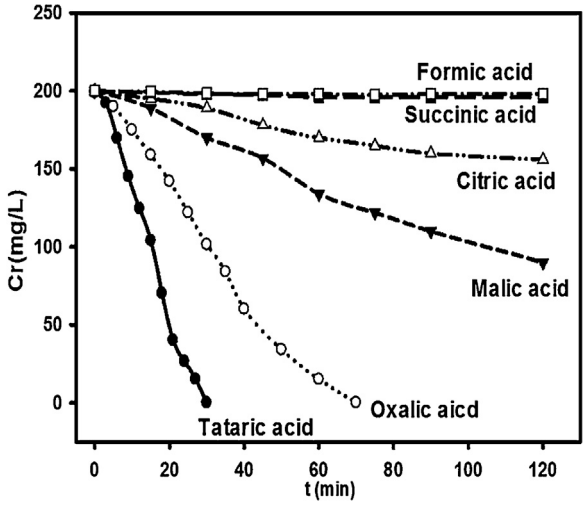

Fig. 2. Photocatalytic reduction of Cr(VI) over TiO_2 nanowire arrays under visible light irradiation in the presence of different LOAs.

chemical structure and the properties of the LOA determine the conversion efficiency of Cr^{VI} to Cr^{III}. This work made a good understanding on the photocatalytic reduction of Cr^{VI} performed under the visible light over TiO_2 in presence of LOAs. Since both TA and Cr^{VI} are necessary reagents during leather making, the theoretical investigation of LOAs assisted surface-catalyzed reduction of Cr^{VI} on TiO_2 will provide an important reference for green reducing of Cr^{VI} from leather manufacture.

2. Materials and methods

2.1. Synthesis of TiO_2 nanowire arrays

TiO_2 NWs were grown on FTO substrate (8 Ω per square, 2cm × 3 cm) through a modified hydrothermal method by referring the reported literature [15,16]. FTO was ultrasonically cleaned in ethanol for 30 min, and deionized (DI) water for 15 min, and was

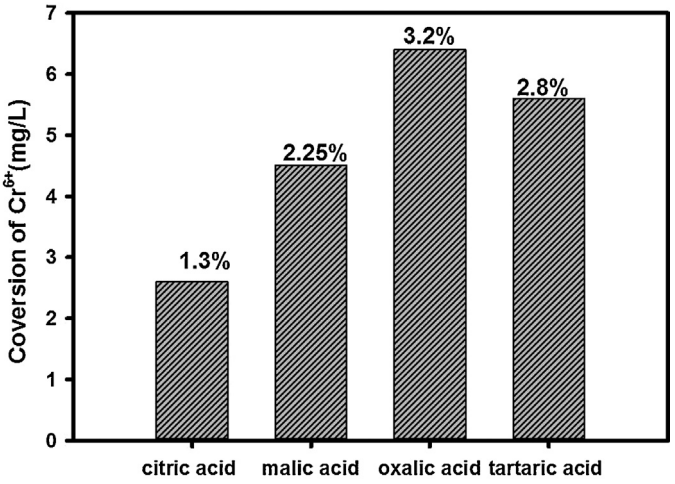

Fig. 3. Comparison between the reduction effects of Cr^{VI} by chemical redox reduction in the LOAs.

dried in air. In order to control the vertical growth of TiO_2 NWs on FTO and improve the adhesion between TiO_2 NWs and FTO, the substrate was seeded with a thin layer of TiO_2 by being calcined in precursor solution at 180 °C for 2 h. After that, FTO substrate loaded with TiO_2 seeds was placed in a new precursor solution and underwent the hydrothermal treatment at same temperature with same duration time for the second time. In a typical synthesis, 2 mL of tetrabutyl titanate (99.9% wt%), 2 mL of titanium tetrachloride (1 M in toluene), and 1 mL of hydrochloric acid (37 wt%) were added dropwise to 10 mL toluene in order in a 25 mL Teflon cell. FTO substrate was placed at an angle of about 45° in the cell. The Teflon cell was sealed and then heated at 180 °C.

2.2. Materials characterizations

Scanning electron microscope (SEM) was performed using a Nova Nano SEM450. Transmission electron microscopy (TEM) analysis was performed using a JEOL 3010. The crystal structure of the catalyst was investigated using the X-ray diffractometer (XRD, M21X, MAC Science Ltd, Japan). Diffuse reflectance spectra (DRS) of the composites were recorded by using a Hitachi U-3010 spectroscopy. X-ray photoelectron spectra (XPS) were recorded with a pressure 2×10^{-9} M bar using Al Ka irradiation (Thermo Fisher Scientific, ESCALAB 250).

2.3. Photocatalytic reduction of Cr^{VI} and analysis

Photocatalytic reduction was carried out in a column quartz reactor. FTO covered with TiO_2 NWs with effectively geometric area of 12 cm^2 was immersed in 60 mL aqueous $K_2Cr_2O_7$ with LOAs. The net weight of TiO_2 NWs peeled from FTO substrates is about 20 mg. The initial concentration of Cr^{VI} was varied in the range of 200–400 mg/L. The visible light is from a 300 W xenon arc lamp (PLS-SXE300C, Beijing Trusttech. Co. Ltd.). A UV-cut filter and an IR cut were settled in the light source to ensure there is no light below 420 nm and no infrared lights. The Xe lamp were irradiated on the side of the reactor by exposing the TiO_2 NWs to the lights. After the photocatalytic experiment was initiated, 0.1 mL volumes of solution were periodically withdrawn from the reaction vessel. Cr^{VI} concentrations were measured using the diphenycarbazide (DPC) method at 540 nm. Every experiment was repeated for 3 times for ensuring the reliability.

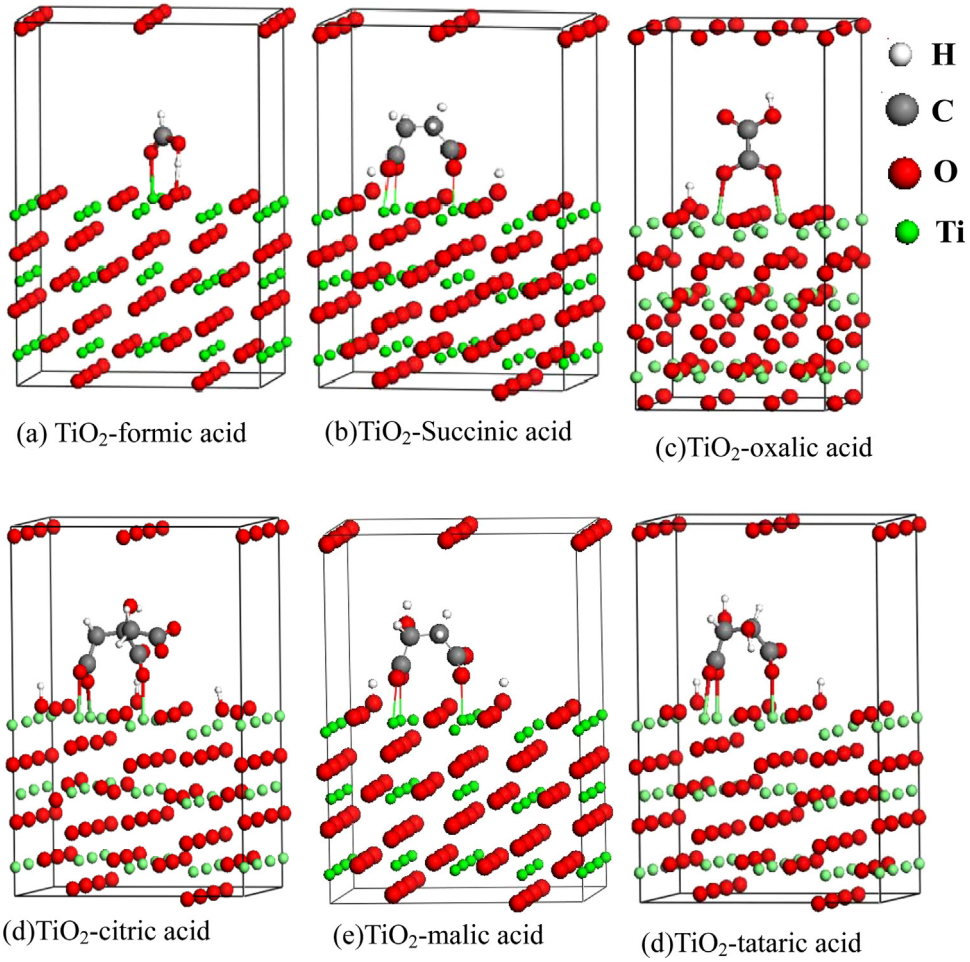

Fig. 4. Representation of the structure of LOA molecule adsorbed molecularly on the rutile (110) terraces. (a) Formic acid, (b) succinic acid, (c) oxalic acid, (d) citric acid, (e) malic acid, and (f) tartaric acid. The vacuum thickness is about 12 Å.

2.4. Computational methods

A DMol^3 molecular orbital package [17] based on the density functional theory (DFT) is used in this simulation process. In aqueous solution, the weak acid (R-OH) tends to dissociate into H^+ and its conjugate base R—O^-. The R—O^- groups from LOAs were bound to Ti atoms and protons to the adjacent O atoms in TiO_2. A vacuum thickness of about 12 Å was used throughout to separate the slabs from their periodic image. During optimization and total energy calculation, electronic exchange-correlation energy functions represented in reciprocal space with the Perdew-Burke-Ernzerh (PBE) of functional type [18], which is based on a generalized gradient approximation (GGA), are employed. All electrons are included in the calculation. Atomic wave functions are developed by double numerical plus d-functions (DND) basis sets [19]. Special K-point method in Monkhorst-Pack scheme [20] is used during the course of Brillouin zone integral. All atomic positions are relaxed according to total energy and force using the BFGS (Broyden, Fletcher, Goldfarb, and Shanno) scheme, based on the geometry optimization criterion ((root-mean-square) RMS force of 0.02 au/Å and RMS displacement of 0.05 Å). The calculation of total energy and electronic structure is followed by the geometry optimization with Self-consistent field (SCF) tolerance of 1×10^{-4} au/atom. The decomposition process of tartaric acid had been calculated by minimum energy path (MEP) embedded in climbing image nudged elastic band (CI-NEB) method [21].

3. Results and discussion

3.1. Morphology and structural characterization of TiO_2 NWs

In Fig. 1a, SEM image shows a top morphology of the as-prepared aligned TiO_2 NWs grown on a FTO substrate, showing the growth of vertical orientation. The NWs will be oriented charge transfer channel in photocatalysis, which are 1.5 μm in length (Fig. 1b) and about 15 nm in diameter (Fig. 1c). The high resolution TEM of a single nanowire in Fig. 1d depicts the spacing of lattice planes which is 0.326 nm corresponding to the (110) plane of rutile [15,16]. The XRD patterns of the as-prepared TiO_2 NWs were supplied in Fig. S1 which also shows the characteristic peaks of rutile.

3.2. Cr^{VI} reduction and adsorption behavior over TiO_2 NWs

Fig. 2 shows the reduction efficiencies of Cr^{VI} on TiO_2 NWs in the presence of FA, OA, SA, MA, CA and TA, respectively. The molar ratio of Cr^{VI}/LOA is about 1/6. All the pH values of the six LOA solutions are tuned to be 3. As the curves shown, when being irradiated by visible light for 60 min, the reduction of Cr^{VI} in FA and SA solutions almost can not occur. In the presence of CA and MA, the conversion efficiencies of Cr^{VI} to Cr^{III} were 25% and 46%, respectively, within 120 min. When OA is used, reducing rate of Cr^{VI} improved to 238 μg/L min cm^2 and complete conversion of Cr^{VI} can be achieved within 70 min. While in TA solution, the highest reducing rate of Cr^{VI} reached 555.5 μg/L min cm^2 and complete

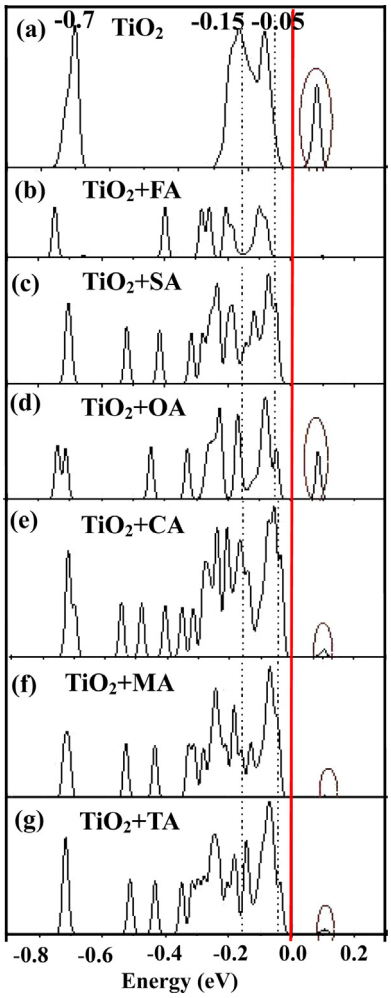

Fig. 5. DOS of TiO_2(110) and TiO_2(110) terraces after adsorbing variable LOAs. (a) TiO_2, (b)TiO_2-Formic acid, (c)TiO_2-Succinic acid, (d)TiO_2—Oxalic acid, (e)TiO_2—Citric acid, (f) TiO_2-Malic acid, and (g) TiO_2-Tartaric acid. The y-axes of (b)-(g) are magnified by a factor of 10 compared to (a). The red line marks the position of E_F (For interpretation of the references to colour in this figure legend, the reader is referred to the web version of this article.)..

reduction is achieved within 30 min. Fig. 3 shows the different chemical reduction effects of Cr^{VI} by different LOAs without the photocatalysts. The experimental results show that Cr^{VI} can not be reduced by FA and SA (Data were not shown) at all. Only about 1.3%, 2.25%, 3.2% and 2.8% of 200 mg/L Cr^{VI} can be converted in the presence of CA, OA and TA at pH 3. The above results suggest that the conversion of Cr^{VI} is very limited without the presence of photocatalysts at pH 3. So the conversion of Cr^{VI} are mainly attributed to the photocatalytic reduction in the presence of TiO_2. This is because at the surface of the TiO_2, the Ti^{4+} will form bonds with oxygen in the LOA and the stability of Ti^{4+}—O bonds will determines the catalytic activity of the TiO_2. It is supposed that the chmisorption of the LOA on TiO_2 is the initial step.

When LOAs were adsorbed onto the surface of TiO_2, due to the Lewis acidity of Ti^{4+} [2,3], it will adsorb the LOAs by accepting the "lone pairs" of the O atoms from the carboxyl groups in the LOAs to form a stable octahedral coordination structure [22–25]. The optimum and most stable adsorption structures of (a) HCOOH (FA), (b) $C_4H_6O_4$ (SA), (c) $C_2H_2O_4$ (OA), (d) $C_6H_8O_7$ (CA), (e) $C_6H_6O_5$ (MA) and (f) $C_4H_6O_6$ (TA) on rutile TiO_2 (110) terraces were depicted in Fig. 4. Among the six LOAs, only FA was bonded to TiO_2 in a mono-dentate coordinated fashion, which is an unstable structure. The

Table 1
Fermi Energy (E_F) of TiO_2, total energy (E_{total}) of TiO_2-LOA system, cohesive energy (Ec) between TiO_2-LOAs.

Model	E_{Total}(eV)	E_c(eV)	E_F(eV)
TiO_2	−55194.6	−2.540	−4.861
TiO_2(110)	−993535.9	−2.848	−5.728
TiO_2(110)-FA	−998707.0	−1.422	−5.722
TiO_2(110)- SA	−1005985.2	−2.824	−5.739
TiO_2(110)-OA	−1003845.9	−2.743	−5.702
TiO_2(110)-CA	−1014243.2	−2.402	−5.598
TiO_2(110)-MA	−1008035.3	−3.400	−5.585
TiO_2(110)-TA	−1010085.5	−3.610	−5.581

other LOAs can coordinate with TiO_2 through a bridged multidentate fashion, which is more stable than the mono-dentate [22].

At low pH, the positively charged TiO_2 supplies an ideal surface for chemi-sorption of LOAs. Those bonds formed between TiO_2 and LOAs have a covalent character. Table 1 lists the calculated results of the total energy (E_{Total}) of TiO_2 (110) after being adsorbed by LOAs. Cohesive energy (E_c) between TiO_2 and the LOAs which identifies the stability of TiO_2-LOA as well as the Fermi level (E_F) of TiO_2 and TiO_2 after being absorbed by LOAs are listed in Table 1. As shown in Table 1, after the LOAs were adsorbed onto the TiO_2, the E_{Total} of TiO_2 increases.

Fig. 5 shows the DOS of TiO_2(110) and TiO_2(110) terraces after being adsorbed with variable LOAs. From the molecular orbital calculations of TiO_2, it is found that, after being adsorbed with LOAs, the double-peak (marked by dotted lines) at −0.15 eV and −0.05 eV respectively in Fig. 5a (which are the bonding molecular orbitals of TiO_2) can be split into multiple peaks as shown in Fig. 5b-g. The intensity of anti-bonding molecular orbital at 0.1 eV significantly decreased. The changes in DOS illustrate that both the band gap and the electric stability of TiO_2 decreased after being adsorbed by the LOAs, indicating that the TiO_2 is in an excited state. However, although all the electronic activities of TiO_2-LOAs are enhanced, the E_F values of them are different. The E_F values of TiO_2-FA and TiO_2-SA are −5.722 eV and −5.739 eV, respectively. They are very close to the −5.728 eV of TiO_2. It is deduced that there is no overlap between TiO_2 LUMO orbitals and FA/SA HOMO orbitals. Consequently, it is difficult for the electrons in FA/SA HOMO orbitals to jump into the orbitals of TiO_2 LUMO (i.e. TiO_2 CB). As to OA, the E_F of TiO_2—OA is −5.702 eV. When adsorbed by the OA molecules, the peak at −0.7 eV representing the bonding molecular orbital of TiO_2 splits into double-peak, which indicates a higher electric activity of TiO_2 in comparison with TiO_2-FA and TiO_2-SA. As a result, the activated TiO_2 can be readily excited by photo and generate electrons in the presence of OA. This is why there is a good Cr^{VI} reduction efficiency in TiO_2—OA system.

As for CA, MA and TA, they are α-hydroxyl carboxylic acids. The DOS plots in Fig. 5e–g show that the intensities of multiple peaks in the range of −0.6–0.0 eV are higher than those in Fig. 5b–d. Furthermore, the E_F of TiO_2—CA, TiO_2-MA and TiO_2-TA is −5.598 eV, −5.585 eV and −5.581 eV, respectively, which is decreased in the order of TiO_2—CA > TiO_2-MA > TiO_2-TA. All the intensity values are lower than that of TiO_2, illustrating that the energy gap between the TiO_2 and the LOAs has been overcome due to the overlap of TiO_2 LUMO and LOA HOMO. The E_F of TiO_2-TA is the lowest among the three acids. It is easiest for TA to transfer electrons to TiO_2 CB. Furthermore, the absolute value of the calculated Ec between TiO_2-LOAs are increased in the order of CA < MA < TA which is consistent with their influence on Cr^{VI} reduction, as depicted in Fig. 2.

Fig. 6 depicts the deformation electron densities of the covalent bond in LOA-TiO_2 species. In the pictures, blue regions are electron-deficient, indicating no bonding there. Yellow regions are charge abundant and have enough bonding electrons. Since TiO_2-FA is in a mono-dentate coordinated fashion (Fig. 4a), which is the most

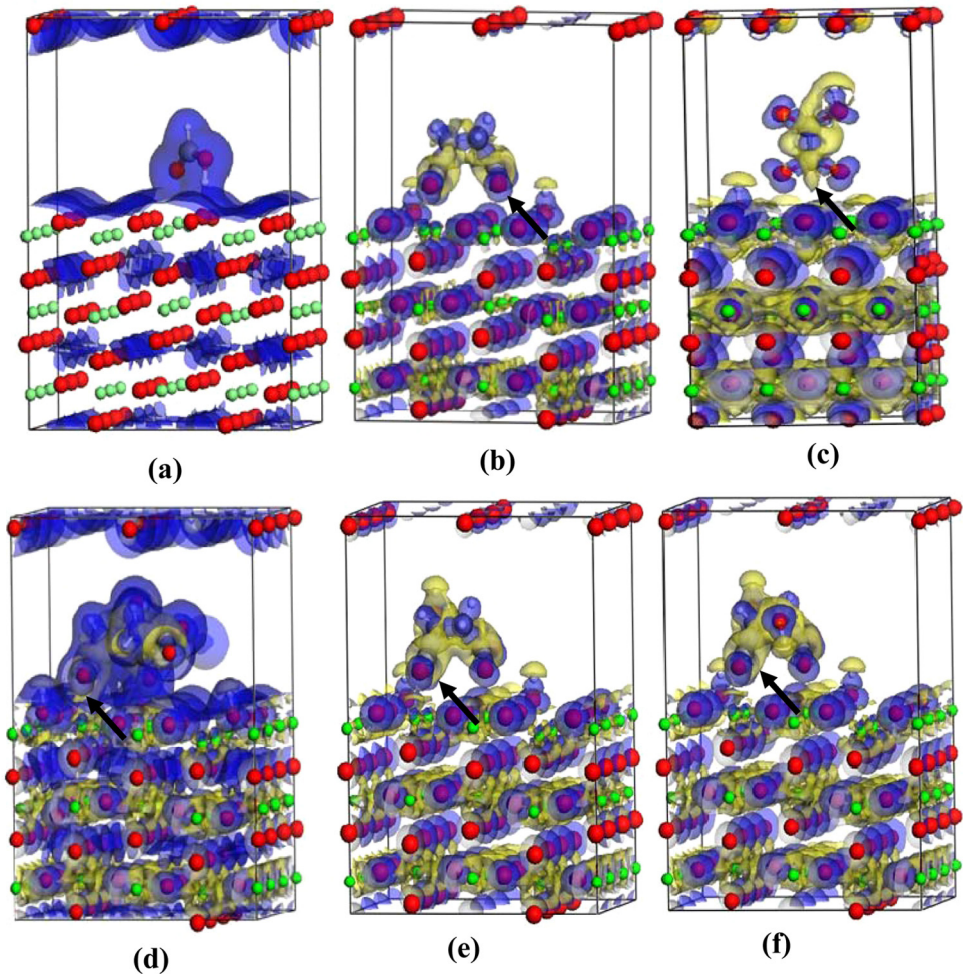

Fig. 6. The deformation electron densities of LOA-TiO_2 species. Blue regions indicate electron-deficient, yellow regions indicate charge-abundant. (a) Formic acid, (b) succinic acid, (c) oxalic acid, (d) citric acid, (e) malic acid, and (f) tartaric acid. The vacuum thickness is about 12 Å (For interpretation of the references to colour in this figure legend, the reader is referred to the web version of this article.).

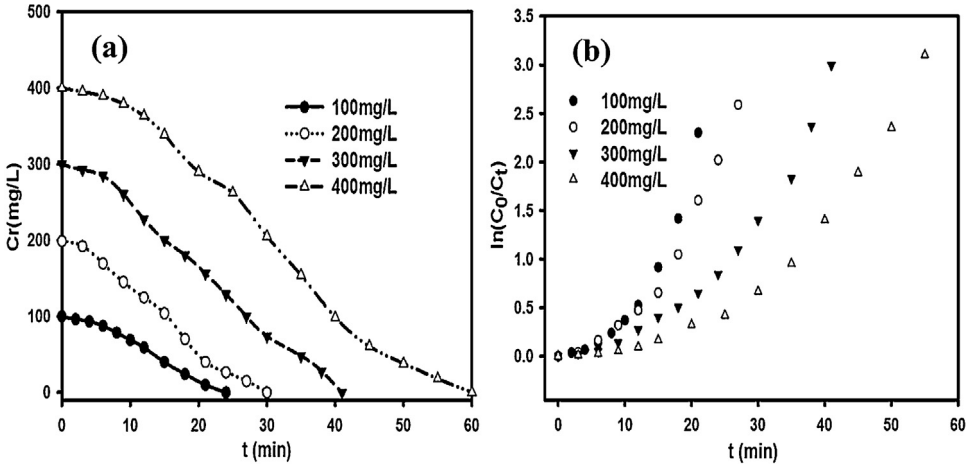

Fig. 7. (a) Effect of initial Cr(VI) concentration on the reduction rate. (b) Plots of $\ln(C_0/C_t)$ versus reaction time.

unstable structure, so only blue region can be seen in Fig. 6a, indicating that there is no bonding between TiO_2-FA. The electrons of FA are difficult to be excited and transferred into TiO_2. As a result, the photocatalytic conversion rate of Cr^{VI} in the presence of FA is low. In Fig. 6b, no yellow regions were observed between SA and TiO_2 as shown by the black arrow, which suggests that no bonding is formed between TiO_2-SA too. For OA, MA, CA and TA, covalent bonds were observed (marked by black arrows in Fig. 6c–f), the deformation electron densities over TiO_2 surface increased in the order of MA < CA < OA < TA.

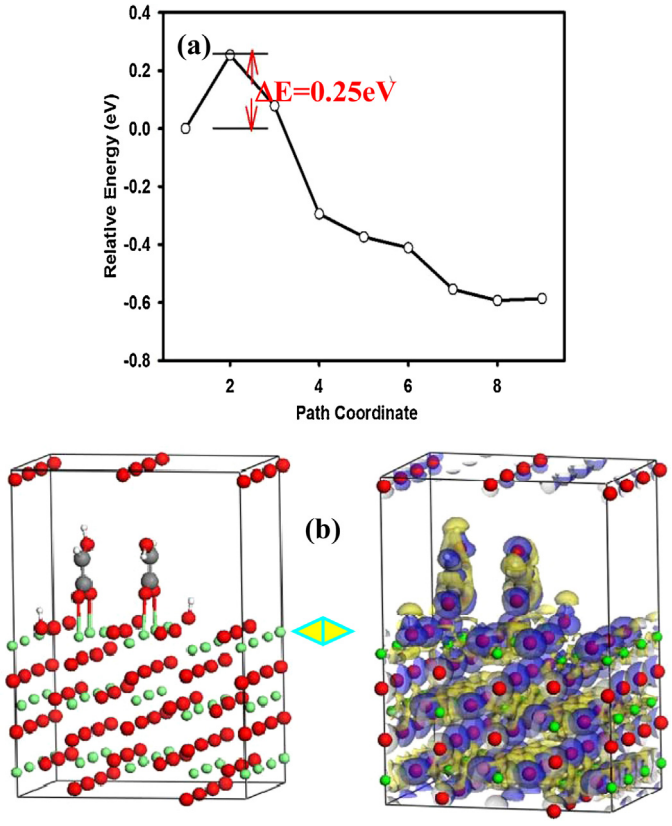

Fig. 8. (a) Demanded energy for TA molecule to split into two segments, (b) adsorption structure of TA segments (TAS) on TiO_2(110) and the corresponding deformation electron densities of TAS-TiO_2. The vacuum thickness is about 12 Å.

3.3. Kinetic model of Cr (VI) reduction irradiated by visible light

Fig. 7a shows the time-evolved photoreduction curves of Cr^{VI} with increased initial concentrations which were conducted at pH 3 in the presence of TA. TiO_2 NWs demonstrate remarkable efficiencies in photocatalytic reduction of high concentration Cr^{VI} solutions. 400 mg/L Cr^{VI} sample can be rapidly detoxified within 60 min. In Fig. 7a, all the photocatalytic reductions of Cr^{VI} follow a tread which is slow at initial stage then get fast in the subsequent stage with initial concentration from 100 to 400 mg. Generally, in a typical heterogeneous photocatalytic process, the temporal evolution of Cr^{VI} concentration (C_t) as a function of time could be correlated to the photocatalytic reduction rate coefficient by the following exponential function.

$$\ln(C_0/C_t) = kt \quad (1)$$

C_0 is the initial concentration of Cr^{VI} solution and k is the observed first-order rate coefficient. The lines in Fig. 7b represent a regression fits to the experimental data set from Fig. 7a, which show us a distinct illustration on the conversion rate of Cr^{VI}. It can be seen that the reaction follow a two-stage first-order dynamics model. Consequently, it is proposed that there are another intermediate species during the photocatalysis. The decomposition process of tartaric acid had been calculated by minimum energy path (MEP) embedded in climbing image nudged elastic band (CI-NEB) method. The NEB method is efficient for finding the MEP between a given initial and final state of a transtion [21]. Firstly, the stable models of TiO_2-TA and TiO_2-TAS were optimized. As Fig. 8a depicted, the energy barrier was calculated according to the initial and final states which correspond to the optimized adsorption geometries obtained before. As shown in Fig. 8a, the energy demanded for the adsorbed TA molecule splitting which is only 0.25 eV, suggesting that it is very easy for TA to be cracked into two segments under the visible light. Fig. 8b shows the adsorption structure of TA segments (TAS) on TiO_2(110) and the corresponding deformation electron densities of TAS-TiO_2. The calculated Ec between TAS and TiO_2 is −4.206 eV. The absolute value is higher than that of TA-TiO_2 (−3.610 eV), suggesting that TAS-TiO_2 is the most stable construction and the electrons in TAS can facilely transfer into TiO_2 CB.

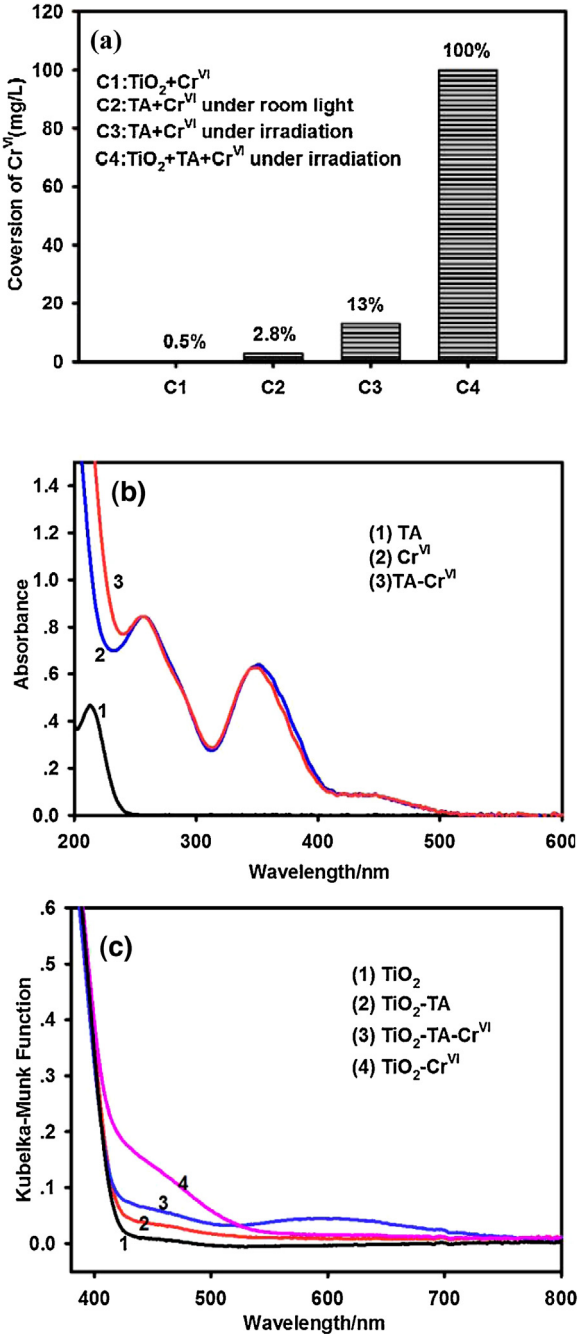

Fig. 9. (a) Comparison of Cr^{VI} removal efficiency in the controlled experiments, and UV–vis absorption (b) and UV–vis diffuse reflectance spectra (c) of single, binary and ternary systems composed of TA, Cr^{VI}, and TiO_2.

As a result, in TA system, two reactions contribute to the Cr^{VI} conversion, the related differential equation is listed below [3]:

$$-d[Cr^{VI}]_T/dt = k_1[Cr^{VI}][TA] + k_2[Cr^{VI}][TAS] \quad (2)$$

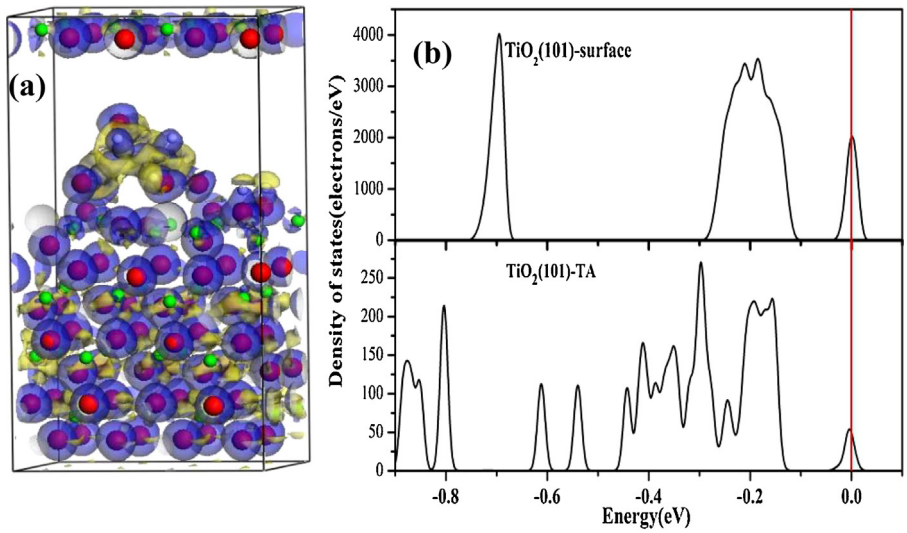

Fig. 10. (a) The deformation electron densities of TA molecule adsorbed on TiO_2 (101) surface, (b) DOS of TiO_2(101) and TiO_2(101) terraces after adsorbing TA. The vacuum thickness is about 12 Å.

Table 2
Rate constants and correlation coefficients of Cr^{VI} conversion in two-stage model with respect to increased initial concentration.

Initial Cr^{VI} Concentration (mg/L)	$K_{1\text{-stage}}$	$K_{2\text{-stage}}$	$R_{1\text{-stage}}$	$R_{2\text{-stage}}$
100	0.017	0.16	0.99	0.98
200	0.015	0.13	0.98	0.98
300	0.0083	0.074	0.99	0.98
400	0.0058	0.067	0.99	0.97

The concentration-dependent rate coefficients and corresponding standard deviations based on Fig. 7b are summarized in Table 2. Rate coefficient $k_{2\text{-stage}}$ values in second stage are almost ten times those of $k_{1\text{-stage}}$ in the starting 10 min. The close fits and the small relative standard deviation supply strong support for the rate law in Eq. (2). As discussed in Figs. 7 and 8, an initial slow decrease in [Cr^{VI}] is caused by TA molecules, while 10 min later, fast decrease in [Cr^{VI}] is caused by the TAS. The above experimental results are in well consistent with the calculated results.

3.4. Proposed mechanisms of Cr^{VI} reduction

To clarify the mechanism of Cr reduction in the presence of TA and TiO_2, controlled experiments under variable experiments noted as C1–C4 were carried out to identify the influence of TiO_2. Furthermore, the UV–vis absorption and UV–vis diffuse reflectance spectra (DRS) of the samples were recorded. The FTO substrate berried with TiO_2 nanowires was immersed into the TA and TA-Cr^{VI} aqueous solution for 30 min and then dried in air for the recording. Related results were shown in Fig. 9.

As Fig. 9a shown, Cr^{VI} can not be converted by TiO_2 without TA (C1). The slight removal of about 0.5% was attributed to the adsorption of Cr^{VI} on TiO_2 nanowires. When TA and Cr^{VI} was mixed in the absence of TiO_2, removal efficiency of Cr^{VI} is 2.8% (C2) and 13% (C3) respectively under room light and irradiation of visible light from the Xe lamp. The conversion of Cr^{VI} in C2 was caused by the chemical reduction between Cr^{VI} and TA. In C3, the enhanced conversion efficiency of 13% through chemical redox may be ascribed to the improved molecular thermal motion under the irradiation. In C4, total removal of Cr^{VI} was achieved by adding TiO_2 nanowires into the TA-Cr system irradiated by the light. The comparison results shown in Fig. 9a identify that the reduction of Cr^{VI} in the presence of TiO_2 and TA is a photocatalytic process.

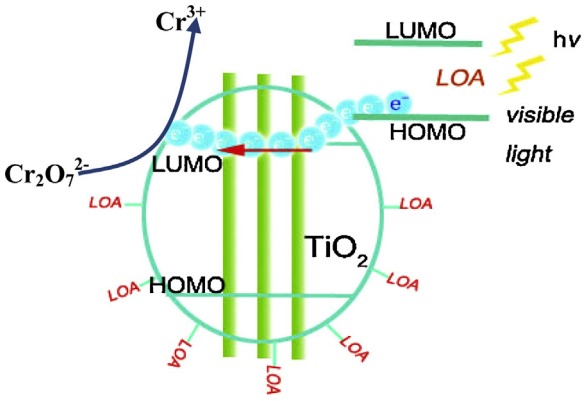

Scheme 1. Proposed schematic illustration of the interfacial charge transfer and Cr^{VI} reduction occurring on TiO_2. LOA represents the surface adsorbed organic acids on TiO_2.

Controlled UV–vis absorption and UV–vis diffuse reflectance spectra (DRS) were recorded to determine the electronic interaction between TiO_2 and TA. As depicted in Fig. 9b, TA can not absorb the visible light. However, as for Cr^{VI} and TA-Cr^{VI} system, two strong UV absorption peak and a weak visible absorption band at about 435 nm were determined. The absorption band at 435 nm is caused by Cr^{VI}. In Fig. 9c, the DRS spectrum of TiO_2 shifts to the visible light region after adsorbing TA molecules (curve 2), which suggests a coordination structure is formed between TA and TiO_2. Especially, a strong visible light absorption band at 600 nm in the TiO_2-TA-Cr^{VI} system (curve 3 in Fig. 9c). This is mainly attributed to the TiO_2-TA species and Cr^{VI}. The above results imply that the ternary TiO_2-TA-Cr system can adsorb visible light and it is a key step for the photocatalytic Cr^{VI} conversion under the irradiation.

In the light of the investigated results and the references [26–29], we propose the possible mechanism of Cr^{VI} reduction carried out by a visible-light sensitive charge-transfer process at the TiO_2 interface as shown in Scheme 1. There are four steps involved in the Cr^{VI} conversion: (1) formation of a coordination complex between the LOAs and the TiO_2 surface, (2) photoexcitation of the absorbed LOA, (3) electrons in the HOMO of the excited LOAs transfer into the TiO_2 LUMO (TiO_2 CB). (4) The electrons from LOAs migrate to the TiO_2 surface through TiO_2 CB (LUMO) and are accepted by $Cr_2O_7^{2-}$, leading to the reduction of Cr^{VI}.

3.5. DOS of TiO_2(101) surface and TiO_2(101)-TA

As shown in Fig. 10a, the structure deformation of TA molecule after being adsorbed on TiO_2 (101) terraces is much more remarkable than that on TiO_2 (110) terraces (Fig. 6f). The calculated E_F of TiO_2 (101) surface is −4.449 eV which is slightly higher than the E_F (−4.480 eV) of TiO_2 (101)-TA. The DOS illustration in Fig. 10b depicts that although TA is adsorbed on the TiO_2 (101) terrace, the energy of the anti-bonding molecular orbital is almost the same with that of E_F, leaving a large band gap below the Fermi level. The above results suggests that there is no overlap area between TiO_2(101) LUMO and TA HOMO, indicating that it is difficult for the electrons in TA HOMO to migrate to TiO_2(101) LUMO. Consequently, it is proposed that TiO_2(110) is the active terrace for TA assisted conversion of Cr^{VI}.

4. Conclusions

This study provides a detailed illustration of Cr^{VI} conversion over TiO_2-based catalysts in the presence of LOAs. Under illumination, the excited LOAs can accelerate the conversion rate by transferring electrons from LOA HOMO to TiO_2 CB through the formation of LOA-TiO_2 species. The formation of LOA-TiO_2 species is the key for the electron transfer. Tartaric acid brings a remarkable influence on accelerating the photocatalytic reduction of Cr^{VI} over TiO_2 nanowire arrays. Usually the tartaric acid exists simultaneously with Cr^{VI} in leather making waste water. It will be an ideal alternative to employ TiO_2 as photocatalyst to replace the conventional techniques that needs expensive chemical reagents to reduce Cr^{VI}.

Acknowledgments

This work is financially supported by the National Natural Science Foundation of China (Grants 51238002, 51272099, 51478214, 51468044), Department of Education fund of Jiangxi Province (Grant GJJ14516), and National Natural Science Foundation of Jiangxi Province (20122BAB203003) are acknowledged.

Appendix A. Supplementary data

Supplementary data associated with this article can be found, in the online version, at http://dx.doi.org/10.1016/j.apcatb.2016.06.002.

References

[1] K. Salnikow, A. Zhitkovich, Chem. Res. Toxicol. 21 (2008) 28–44.
[2] B.L. Deng, A.T. Stone, Environ. Sci. Technol. 30 (1996) 2484–2494.
[3] B.L. Deng, A.T. Stone, Environ. Sci. Technol. 30 (1996) 463–472.
[4] J.J. Testa, M.A. Grela, M.I. Litter, Environ. Sci. Technol. 38 (2004) 1589–1594.
[5] B. Sun, E.P. Reddy, P.G. Smirniotis, Environ. Sci. Technol. 39 (2005) 6251–6259.
[6] G. ColÓn, M.C. Hidalgo, J.A. NavÍO, Langmuir 17 (2001) 7174–7177.
[7] Y.C. Zhang, M. Yang, G.S. Zhang, D.D. Dionysiou, Appl. Cata. B: Environ. 142–143 (2013) 249–258.
[8] G. Kim, W.-Y. Choi, Appl. Catal. B: Environ. 100 (2010) 77–83.
[9] N. Wang, L.H. Zhu, K.J. Deng, Y.B. She, Y.M. Yu, H.Q. Tang, Appl. Catal. B: Environ. 95 (2010) 400–407.
[10] R.L. Qiu, D.D. Zhang, Z.H. Diao, X.F. Huang, C. He, J.L. Morel, Y. Xiong, Water Res. 46 (2012) 2299–2306.
[11] J. Kuncewicz, P. Zabek, K. Kruczala, K. Szacilowski, W. Macyk, J. Phys. Chem. C 116 (2012) 21762–21770.
[12] J. Schneider, M. Matsuoka, M. Takeuchi, J.L. Zhang, Y. Horiuchi, M. Anpo, D.W. Bahnemann, Chem. Rev. 114 (2014) 9919–9986.
[13] F.D. Angelis, C.D. Valentin, S. Fantacci, A. Vittadini, A. Selloni, Chem. Rev. 114 (2014) 9708–9753.
[14] K. Bourikas, C. Kordulis, A. Lycourghiotis, Chem. Rev. 114 (2014) 9754–9823.
[15] X.J. Feng, K. Shankar, O.K. Varghese, M. Paulose, T.J. Latempa, C.A. Grimes, Nano Lett. 8 (2008) 3781–3786.
[16] A. Kumar, A.R. Madaria, C.W. Zhou, J. Phys. Chem. C 114 (2010) 7787–7792.
[17] B. Delley, J. Chem. Phys. 113 (2000) 7756–7764.
[18] S.H. Vosko, L. Wilk, M. Nusair, Can. J. Phys. 58 (1980) 1200–1211.
[19] B. Delley, J. Chem. Phys. 94 (1991) 7245–7250.
[20] D. Pack, H.J. Monkhorst, Phys. Rev. B 16 (1977) 1748–1749.
[21] G. Henkelman, B.P. Uberuage, H. Jonsson, J. Chem. Phys. 113 (2000) 9978–9985.
[22] S. Tunesi, M. Anderson, J. Phys. Chem. 95 (1991) 3399–3405.
[23] P. Persson, R. Bergström, S. Lunell, J. Phys. Chem. B 104 (2000) 10348–10351.
[24] L. Pattery, H. Rensmo, P. Persson, K. Westermark, L. Vayssieres, A. Stashans, Å. Petersson, P.A. Brühwiler, H. Siegbahn, S. Lunell, N. Mårtensson, J. Chem. Phys. (1999) 5913–5918.
[25] C.L. Pang, R. Lindsay, G. Thornton, *2013*, Chem. Rev. 113 (*2013*) 3887–3948.
[26] T. Paul, P.L. Miller, T.J. Sterathmann, Environ. Sci. Technol. 41 (2007) 4720–4727.
[27] E.R. Travis, N.K. Hannink, C.J. van der Gast, I.P. Thompson, S.J. Rosser, N.C. Bruce, Environ. Sci. Technol. 41 (2007) 5854–5861.
[28] N. Wang, L.H. Zhu, Y.P. Huang, Y.B. She, Y.M. Yu, H.Q. Tang, J. Catal. 266 (2009) 199–206.
[29] N. Wang, L.H. Zhu, K.J. Deng, Y.B. She, Y.M. Yu, H.Q. Tang, Appl. Catal. B: Environ. 99 (2010) 400–407.